Materials Horizons

ROYAL SOCIETY OF CHEMISTRY

COMMUNICATION

View Article Online
View Journal | View Issue

Cite this: *Mater. Horiz.*, 2023, **10**, 3450

Received 17th April 2023,
Accepted 5th June 2023

DOI: 10.1039/d3mh00572k

rsc.li/materials-horizons

Ferroelectrically tunable magnetic skyrmions in two-dimensional multiferroics†

Zhonglin He, Wenhui Du, Kaiying Dou, Ying Dai, * Baibiao Huang and Yandong Ma *

Magnetic skyrmions are topologically protected entities that are promising for information storage and processing. Currently, an essential challenge for future advances of skyrmionic devices lies in achieving effective control of skyrmion properties. Here, through first-principles and Monte-Carlo simulations, we report the identification of nontrivial topological magnetism in two-dimensional multiferroics of Co_2NF_2. Because of ferroelectricity, monolayer Co_2NF_2 exhibits a large Dzyaloshinskii–Moriya interaction. This together with exchange interaction can stabilize magnetic skyrmions with the size of sub-10 nm under a moderate magnetic field. Importantly, arising from the magnetoelectric coupling effect, the chirality of magnetic skyrmions is ferroelectrically tunable, producing the four-fold degenerate skyrmions. When interfacing with monolayer $MoSe_2$, the creation and annihilation of magnetic skyrmions, as well as phase transition between skyrmion and skyrmion lattice, can be realized in a ferroelectrically controllable fashion. A dimensionless parameter κ' is further proposed as the criterion for stabilizing magnetic skyrmions in such multiferroic lattices. Our work greatly enriches the two-dimensional skyrmionics and multiferroics research.

New concepts

Magnetic skyrmions have attracted increasing attention recently. To translate the compelling features of magnetic skyrmions into practical spintronic devices, it is crucial to achieve effective control of skyrmion properties, including density and morphology. Electric field *via* ferroelectric switching has been considered as a very efficient method, which can significantly reduce energy consumption. Nonetheless, the *in situ* ferroelectric control of skyrmion properties in 2D systems remains challenging. Herein, we report the discovery of topological magnetism in 2D multiferroics of Co_2NF_2. Arising from strong spin-orbit coupling and inversion symmetry breaking, a large DMI occurs in monolayer Co_2NF_2. This competing with ferromagnetic Heisenberg exchange interaction can stabilize magnetic skyrmions under a moderate magnetic field, with the size of sub-10 nm. Due to the magnetoelectric coupling effect, the switching of chirality of magnetic skyrmions is realized in monolayer Co_2NF_2 in a ferroelectrically controllable fashion, which yields the four-fold degenerate skyrmions. By interfacing with monolayer $MoSe_2$, the ferroelectrically controllable creation-annihilation of magnetic skyrmions, as well as phase transition between skyrmion and skyrmion lattice, are obtained.

Magnetic skyrmions are whirling spin textures exhibiting nontrivial topology in real space.[1] Each skyrmion is characterized by a topological invariant $Q = \pm 1$ that measures the winding of the normalized local magnetization, **m**. This chiral spin configuration can be stabilized as a result of competing Heisenberg exchange interaction and Dzyaloshinskii–Moriya interaction (DMI).[2–4] Since their first observation in B20 bulk MnSi[5] and thin film $Fe_{0.5}Co_{0.5}Si$,[6] magnetic skyrmions have attracted tremendous attention because of a variety of intriguing characteristics, such as topological robustness against continuous deformation, self-organized lattice form, and solitonic nature with current-driven motion.[7–11] These exotic properties not only open up new opportunities for exploring nontrivial topological

Yandong Ma

Our first paper was published in Materials Horizons in 2019, and more than 7 papers have been published in Materials Horizons in these 4 years. We are proud to have so long a history in cooperation with such an excellent journal. We think the best way to express our gratitude is to continue to report our significant research advances such as this newly discovered ferroelectrically tunable magnetic skyrmions in two-dimensional multiferroics. We would like to further contribute this journal. Congratulations on the 10th anniversary and best wishes to the Materials Horizons.

School of Physics, State Key Laboratory of Crystal Materials, Shandong University, Shandanan Street 27, Jinan 250100, China. E-mail: daiy60@sina.com, yandong.ma@sdu.edu.cn

† Electronic supplementary information (ESI) available. See DOI: https://doi.org/10.1039/d3mh00572k

physics but also hold high potential for applications in future spintronics devices.[12–14] Apart from conventional cubic B20 bulk crystals[6] and thin films,[15–17] in recent experiments, two independent groups have reported the observation of magnetic skyrmions in the van der Waals magnets Cr_2GeTe_6[18] and Fe_3GeTe_2,[19] rendering two-dimensional (2D) magnetic materials a new category of skyrmion medium.[20–25]

To translate the compelling features of magnetic skyrmions into practical spintronic devices, it is crucial to achieve effective control of skyrmion properties, including density and morphology.[26–28] For bulk compounds, the magnetic interactions are almost invariant. In contrast, magnetic skyrmions in heavy-metal/ferromagnet thin films are sensitive to various external stimuli, such as spin-transfer torque,[29] electric field,[30] and current gradient.[31] Among them, electric field *via* ferroelectric (FE) polarization switching is considered a more effective method, which can significantly reduce energy consumption. Nonetheless, the *in situ* ferroelectric control of skyrmion properties in 2D systems remains challenging.[32–34] Recently, 2D multiferroics, which simultaneously exhibit ferroelectricity and magnetism, have received increasing interest.[35,36] In 2D multiferroic materials, the intrinsic inversion symmetry breaking gives rise to DMI, while the time-reversal symmetry breaking guarantees Heisenberg exchange interaction[34]. This quite naturally provides the possibility for the formation of magnetic skyrmions. Furthermore, through the magnetoelectric coupling effect, ferroelectrically tunable magnetic skyrmions are highly anticipated in such systems.

Here, based on first-principles calculations and Monte-Carlo (MC) simulations, we report the discovery of topological magnetism in 2D multiferroics of Co_2NF_2. Arising from strong spin-orbit coupling (SOC) and inversion symmetry breaking, a large DMI occurs in monolayer Co_2NF_2. This competing with ferromagnetic (FM) Heisenberg exchange interaction can stabilize magnetic skyrmions under a moderate magnetic field, with the size of sub-10 nm. Due to the magnetoelectric coupling effect, the switching of chirality of magnetic skyrmions is realized in monolayer Co_2NF_2 in a ferroelectrically controllable fashion, which yields the four-fold degenerate skyrmions. By interfacing with monolayer $MoSe_2$, the ferroelectrically controllable creation-annihilation of magnetic skyrmions, as well as phase transition between skyrmion and skyrmion lattice, are obtained. Furthermore, we also unveil a dimensionless parameter κ' as the criterion for assessing the formation of magnetic skyrmions in such multiferroic lattices. This work thus provides a novel avenue toward the design and control of magnetic skyrmions on 2D multiferroics.

Fig. 1(a and b) show the crystal structure of monolayer Co_2NF_2. It exhibits a hexagonal lattice with $P3m1$ space group, and is composed of five triangular atomic layers stacked in the sequence of F-Co1-N-Co2-F. The lattice constant is optimized to be 2.87 Å, which agrees well with the previous work.[37] To assess the stability of Co_2NF_2, we first calculate its phonon spectra. As shown in Fig. S1(a) (ESI†), except for the tiny imaginary frequencies around the Γ point, all branches are positive, suggesting the dynamical stability. The thermal stability of monolayer Co_2NF_2 is also investigated using *ab initio* molecular dynamics (AIMD) simulations. As illustrated in Fig. S1(b) (ESI†), after heating at 500 K for 5 ps, neither structure reconstruction nor bond breaking is found, which confirms that it is thermally stable as well.

In Co_2NF_2, as shown in Fig. 1(b), the N atomic layer favors a vertical displacement with respect to the central horizontal

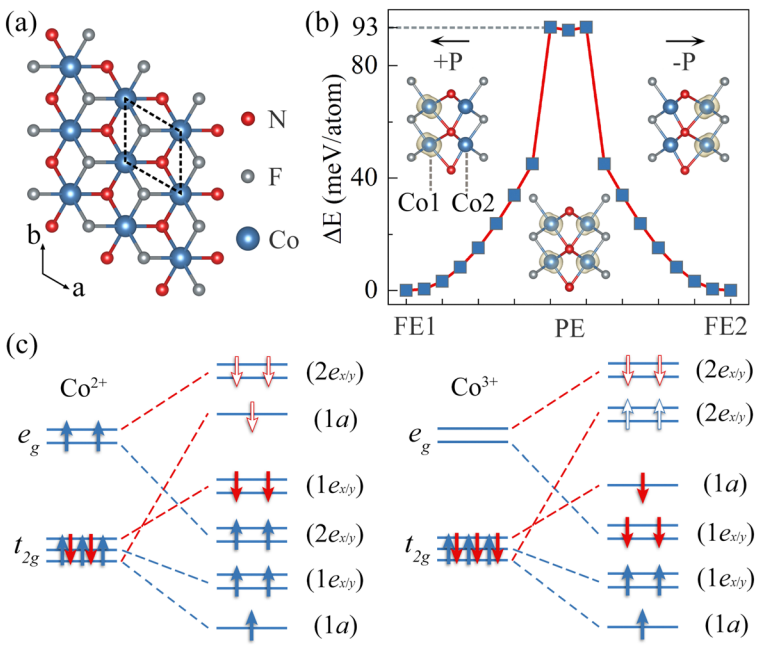

Fig. 1 (a) Crystal structure of monolayer Co_2NF_2 from top view, with the dashed diamond indicating the unit cell. (b) Minimum energy path for FE transition in monolayer Co_2NF_2. Insets in (b) show the crystal structures of the FE and paraelectric (PE) phases for monolayer Co_2NF_2, wherein the spin charge density is represented by yellow isosurfaces. (c) Schematic diagrams of the d orbital occupations for Co atoms.

plane of Co dimers. This breaks the inversion symmetry and leads to an out-of-plane (OP) electric polarization. As the N atom can move vertically towards either Co1 or Co2 atoms and these two vertical displacements are energetically equivalent, the resulting two configurations can be considered as two FE states. To guarantee FE order in Co_2NF_2, we calculate the minimum energy path for the ferroelectric switching. The corresponding energy barrier is estimated to be 93 meV per atom, comparable to those of $CuAP_2S_6$ (A = In, Bi),[38] SnX (X = S, Se),[39] and Sc_2CO_2.[40] This suggests the feasibility of ferroelectricity in Co_2NF_2. In addition to FE order, Co_2NF_2 prefers a spin-polarized phase with a magnetic moment of $3\mu_B$ per unit cell. From the spin charge density shown in Fig. 1(b), we can see that the magnetic moment is mainly distributed on the Co atom lying further from the N atom, while another Co atom has no contribution to the magnetic moment. In this regard, the magnetic moment can be exchanged between the two Co atoms through ferroelectric transition, indicating that Co_2NF_2 is a multiferroic material with strong magnetoelectric coupling. For convenience of discussion, unless otherwise stated, Co_2NF_2 refers to the FE1 phase in the following.

To get insight into the magnetoelectric coupling in Co_2NF_2, we investigate the origin of its magnetism. The valence electronic configuration of the Co atom is $3d^74s^2$. For the Co1 atom, it donates one valence electron to the surrounding N and F atoms, giving rise to the oxidation state of +2. Different from the Co1 atom, the vertical displacement of the N atom strengthens its bonding with Co2. As a result, the Co2 atom donates one more valence electron to the N atom compared with the Co1 atom, and thus possesses an oxidation state of +3. Under the octahedral crystal field, the *d* orbitals split into two manifolds, *i.e.*, the higher doublet e_g orbitals and the lower triplet t_{2g} orbitals. As shown in Fig. 1(b), due to the distortion of the octahedral geometry and magnetic exchange field, e_g and t_{2g} orbitals further split. Because of the vertical displacement of the N atoms, the resulting orbitals are different for the Co1 and Co2 atoms, which is consistent with the projected density of states (PDOS) in Fig. S3 (ESI†). According to Hund's rule and the Pauli exclusion principle, the electronic configuration of $Co1^{2+}$ is $t_{2g}^5e_g^2$, generating a magnetic moment of $3\mu_B$ per Co1 atom, as shown in Fig. 1(c). While for $Co2^{3+}$, the electronic configuration is $t_{2g}^6e_g^0$, suggesting the absence of a magnetic moment. Under ferroelectric transition, the coordination environments as well as the number of transferred electrons for Co1 and Co2 atoms are exchanged, which is accompanied by the exchange of magnetic moments on them. With these results in hand, we can easily understand the magnetoelectric coupling in Co_2NF_2.

For further exploring the magnetic properties of Co_2NF_2, we introduce a Heisenberg spin Hamiltonian:

$$H = -J\sum_{\langle i,j\rangle}(\mathbf{m}_i\cdot\mathbf{m}_j) - \lambda\sum_{\langle i,j\rangle}\left(\mathbf{m}_i^z\cdot\mathbf{m}_j^z\right) - K\sum_{\langle i\rangle}(\mathbf{m}_i^z)^2 - \mu_{Mn}B\sum_{\langle i\rangle}\mathbf{m}_i^z - \sum_{\langle i,j\rangle}\boldsymbol{D}_{ij}\cdot(\mathbf{m}_i\times\mathbf{m}_j). \quad (1)$$

Here, $\mathbf{m}_i$ is normalized spin vector ($|\mathbf{m}_i| = 1$) representing the local magnetic moment at the *i*th Co atom, and the OP component of $\mathbf{m}_i$ is denoted by $\mathbf{m}_i^z$. The summation $\langle i\rangle$ runs over all magnetic Co sites and $\langle i,j\rangle$ runs over all nearest neighbor (NN) magnetic Co pairs. The Heisenberg model includes NN isotropic exchange, NN anisotropic symmetric exchange, magnetic anisotropy, external magnetic field and DMI, which are described by J, λ, K, B and $\boldsymbol{D}_{ij}$, respectively. Magnetic anisotropy K is composed of two parts: one is the single ion anisotropy K_C and the other is the shape anisotropy K_S. For 2D FM systems, K_S, which is determined by the locations and magnetic moments of magnetic atoms, favors in-plane (IP) magnetization.[41] The obtained magnetic parameters are listed in Table S1 (ESI†). The positive J indicates that FM coupling is favorable for the isotropic exchange interaction between NN magnetic Co atoms. According to the Goodenough–Kanamori–Anderson mechanism,[42–44] such FM coupling is related to the Co–F–Co bonding angle of $\sim 90^\circ$. The magnetization orientation is determined by the combined effects of λ, K_S and K_C. As shown in Table S1 (ESI†), the positive K_C is much larger than the negative λ and K_S, indicating that the easy magnetization axis is along the OP direction for Co_2NF_2.

According to the Moriya's rule[45], the DMI vector can be simplified as $\boldsymbol{D}_{ij} = d_\parallel(\boldsymbol{u}_{ij}\times z) + d_z z$, where $\boldsymbol{u}_{ij}$ and z are the unit vector from site i to j and along the z direction. In view of the C_{3v} symmetry, the OP component d_z is arranged in a staggered pattern, rendering it negligible in Co_2NF_2.[20,22] We therefore only consider the IP component $d_\parallel$ of the DMI vector. To obtain $d_\parallel$, we consider two spin-spiral configurations, *i.e.*, the clockwise (CW) and anticlockwise (ACW) configurations (see Fig. S4(a), ESI†). The $d_\parallel$ is calculated to be -1.01 meV. Based on the layer-resolved SOC energy difference (ΔE) between the two spin-spiral configurations shown in Fig. 2(a), it can be seen that ΔE is mainly contributed by the magnetic Co1 atom, which suggests that the DMI is dominated by the Rashba effect in Co_2NF_2. In addition to the magnetic Co1 atom, there is a moderate DMI contribution from the nonmagnetic Co2 atom, that is, the nonmagnetic Co2 atom also acts as a SOC-active site to induce spin-orbit scattering necessary for DMI, corresponding to the Fert–Levy mechanism.[49] Therefore, the Fert–Levy mechanism also plays a nonnegligible role for forming DMI in Co_2NF_2. We wish to point out that different from the scalar magnetic parameters, the chirality of DMI vector $\boldsymbol{D}_{ij}$ is tunable under FE transition. For example, when switching to the FE2 state, the sign of the IP component of the DMI vector is reversed, *i.e.*, $d_\parallel = 1.01$ meV.

Concerning the NN isotropic exchange interaction and DMI of Co_2NF_2, the ratio between them is estimated to be $|d_\parallel/J| = 0.28$. Note that $0.1 < |d_\parallel/J| < 0.2$ is usually considered as a criterion to stabilize magnetic skyrmions.[20,22] The large $|d_\parallel/J|$ suggests the existence of spin spiral states (SS) in Co_2NF_2, which might transform into skyrmion lattice (SkL) phase through applying an external magnetic field.[46] Notably, different from the skyrmion (SkX) phase that consists of isolated magnetic skyrmions, the SkL phase is composed of regular arrays of magnetic skyrmions. To verify this possibility, based

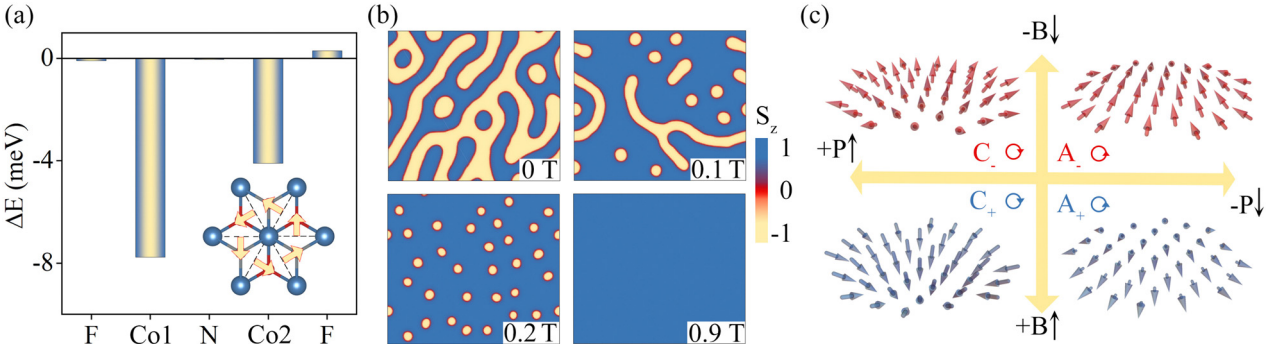

Fig. 2 (a) Atomic-resolved localization of DMI associated SOC energy (ΔE) for Co_2NF_2. Inset illustrates the DMI vectors (yellow arrows) between the nearest-neighboring Co atoms. (b) Spin textures of Co_2NF_2 under a magnetic field of 0, 0.1, 0.2 and 0.9 T. Color map in (b) specifies the OP spin component. (c) The interconversion diagram for the core part of the four-fold degenerate skyrmions. In (c), topological charge Q is denoted by the subscripts "±", and the chirality γ = + 1/−1 isdistinguished by characters A/C (ACW/CW) and the rotating circular arrows.

on the magnetic parameters obtained from first-principles calculations, we perform the parallel tempering MC simulations to explore the spin textures in Co_2NF_2. Here, we introduce topological charge Q to characterize the nontrivial property of magnetic skyrmions, which is given by[47]

$$Q = \frac{1}{4\pi}\sum_n q_n. \quad (2)$$

Here, $\tan\frac{q_n}{2} = \frac{\boldsymbol{S}_i^n \cdot \left(\boldsymbol{S}_j^n \times \boldsymbol{S}_k^n\right)}{1 + \boldsymbol{S}_i^n \cdot \boldsymbol{S}_j^n + \boldsymbol{S}_j^n \cdot \boldsymbol{S}_k^n + \boldsymbol{S}_k^n \cdot \boldsymbol{S}_i^n}$. $\boldsymbol{S}_i^n$, $\boldsymbol{j}_i^n$ and $\boldsymbol{k}_i^n$ are the three spin vectors of the nth equilateral triangle in the ACW lattice. The spin texture of Co_2NF_2 under zero magnetic field is illustrated in Fig. 2(b). Intriguingly, although the ratio $|d_\parallel/J|$ is rather large, the isolated Néel-type magnetic skyrmions with nontrivial topological $Q = \pm 1$ is still observed near the labyrinth domains (see Fig. S4(b), ESI†). Such unexpected emergency of magnetic skyrmions in Co_2NF_2 under zero magnetic field can be attributed to its large magnetic anisotropy, which enhances the collinear spin arrangement.[22,48] Moreover, the diameters of these magnetic skyrmions are found to be only ∼8 nm, which is highly desirable for device applications.

We then study the effect of an external magnetic field on the topological spin textures of Co_2NF_2. From Fig. 2(b) we can see that with increasing magnetic field from 0 to 0.1 T, the labyrinth domains shrink and more magnetic skyrmions emerge. When applying a magnetic field of 0.2 T, the labyrinth domains disappear completely, resulting in isolated magnetic skyrmions with $Q = 1$ embedded in the FM background. In this regard, the intriguing skyrmion (SkX) phase is realized in Co_2NF_2. Remarkably, the SkX phase can be preserved within a wide range of 0.2–0.9 T. Upon further increasing the magnetic field, the SkX phase transforms into the trivial FM phase. Therefore, except for the intriguing SkX phase, the expected SkL phase is absent in Co_2NF_2, which also results from its large magnetic anisotropy. Along with the evolution of topological spin textures, the diameter of the magnetic skyrmion is reduced with increasing the magnetic field. This phenomenon correlates to the fact that the magnetic field prefers to align spins. As for the density of magnetic skyrmions, as shown in Fig. S4(c) (ESI†), it first increases with the magnetic field and achieves the maximum of ∼0.05 per nm^2 (44 per supercell) under the magnetic field of 0.5–0.65 T; with further increasing the magnetic field (0.65–0.9 T), it decreases rapidly and shrinks down to zero at 0.9 T, which corresponds to the trivial FM phase.

For the magnetic skyrmions in Co_2NF_2, as shown in Fig. 2(b), the core spin aligns antiparallel to the external magnetic field. With reversing the magnetic field, the core spin orientation of the magnetic skyrmions can be reversed, which would switch the signs of the topological charge, *i.e.*, Q and -Q. Besides, as we mentioned above, the chirality of DMI vector $\boldsymbol{D}_{ij}$ in Co_2NF_2 can be reversed under FE transition. As the chirality γ of the magnetic skyrmion is locked by the sign and direction of the DMI vector, the chirality of magnetic skyrmions in Co_2NF_2 is ferroelectrically controllable, *i.e.*, γ and -γ. Based on these properties, the four-fold degenerate Néel-type magnetic skyrmions with $(Q, \gamma) = (\pm 1, \pm 1)$ are realized in Co_2NF_2, and these four states can be transformed into each other through FE and FM inversion, as illustrated in Fig. 2(c).

Considering the particular structure of Co_2NF_2, we propose a mechanism of coupling its multiferroics with a nonmagnetic substrate for realizing FE control of more skyrmion properties. We select monolayer $MoSe_2$ as the nonmagnetic substrate and construct the $Co_2NF_2/MoSe_2$ heterobilayer. Due to the significant difference in electronegativity between Se and F atoms, $Co_2NF_2/MoSe_2$ is expected to exhibit a relatively strong interlayer coupling. This can lead to significant difference between the two FE states of Co_2NF_2, which is beneficial for enhancing the FE control of skyrmion properties. In $Co_2NF_2/MoSe_2$, a $\sqrt{3} \times \sqrt{3}$ supercell of $MoSe_2$ is used to match a 2 × 2 supercell of Co_2NF_2, which results in a rather small lattice mismatch of less than 1%. The binding energy of $Co_2NF_2/MoSe_2$ as a function of normalized interlayer sliding is summarized in Fig. 3(a). We can see that the structure with N lying vertically above the Mo atom is the most stable configuration. In the following, we only consider this configuration (see Fig. S5ESI†). By interfacing with $MoSe_2$, an interface dipole $\mathbf{P}_i$ pointing from $MoSe_2$ to

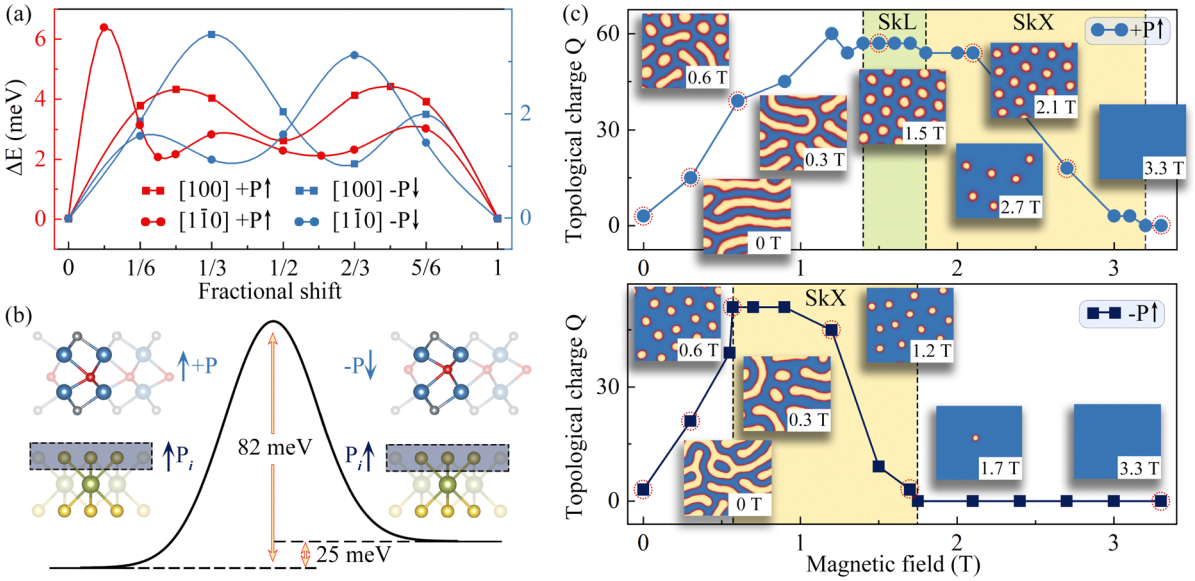

Fig. 3 (a) Binding energy of the $Co_2NF_2/MoSe_2$ heterobilayer with respect to the N-Mo stacking configuration as a function of normalized interlayer sliding. The N-Mo stacking configuration corresponds to the N atom from Co_2NF_2 lying vertically above the Mo atom from $MoSe_2$. (b) Minimum energy path for the transition between FE1 (+P↑) and FE2 (−P↓) phases of $Co_2NF_2/MoSe_2$. Insets in (b) show the crystal structures of the +P↑ and −P↓ phases. $\mathbf{P}_i$ represents the external dipole caused by the interface. (c) Evolutions of topological charge Q and spin textures of $Co_2NF_2/MoSe_2$ as functions of magnetic field.

Co_2NF_2 is generated due to the different electronegativities of the interfaced atoms. The interface dipole $\mathbf{P}_i$ would interact with the FE polarization $\mathbf{P}$, forming a dipole–dipole interaction in the form of $-a\mathbf{P}\cdot\mathbf{P}_i/r^3$, where a is a constant and r is the distance between the two dipoles. Clearly, the FE1 phase with $\mathbf{P}$ parallel to $\mathbf{P}_i$ tends to be lower in energy than FE2 with $\mathbf{P}$ antiparallel to $\mathbf{P}_i$; see Fig. 3(b). And thus, the degeneracy of the two FE states is lifted in $Co_2NF_2/MoSe_2$. As shown in Fig. 3(b), the FE switching barriers from FE1 (+P↑) to FE2 (−P↓) and FE2 (−P↓) to FE1 (+P↑) phases are calculated to be 82 and 57 meV per atoms, respectively. These values are lower than that of freestanding Co_2NF_2, guaranteeing the feasibility of the FE order in $Co_2NF_2/MoSe_2$.

Based on eqn (1), we calculate the magnetic parameters of these two FE states (+P↑ and −P↓) of $Co_2NF_2/MoSe_2$ (see Table S1ESI†). It can be seen that, as compared with free-standing Co_2NF_2, K_C for both +P↑ and −P↓ are substantially weakened (see ESI† for more details), while J and $d_\parallel$ vary slightly. Based on these magnetic parameters, we conduct the parallel tempering MC simulations to investigate the spin textures of $Co_2NF_2/MoSe_2$. Fig. 3(c) illustrates the evolutions of topological charge Q and spin textures of +P↑ and −P↓ as functions of magnetic field. It can be seen that +P↑ favors the SS phase under zero magnetic field. With increasing magnetic field, the labyrinth domains disappear and transform into SkL phase under 1.4–1.8 T. Upon increasing the magnetic field to 1.8–3.2 T, the ordered array of magnetic skyrmions is disrupted and SkX phase forms. Under the magnetic field larger than 3.2 T, the spin textures of +P↑ show a trivial FM phase. Different from +P↑, as shown in Fig. 3(c), isolated Néel-type magnetic skyrmions are observed near the labyrinth domains for −P↓ under zero magnetic field. When applying a magnetic field, the labyrinth domains shrink and more magnetic skyrmions emerge. Under 0.6–1.75 T, the labyrinth domains vanish completely and the SkX phase is favorable for −P↓. Upon increasing the magnetic field larger than 1.75 T, −P↓ prefers the trivial FM phase. Because these two FE states favor different topological spin textures under a magnetic field, the effective control of more skyrmion properties in a ferroelectrically controllable fashion is realized in $Co_2NF_2/MoSe_2$. For example, the creation and annihilation of magnetic skyrmions is ferroelectrically controllable under 0.6–1.4 and 1.75–3.2 T, while under 1.4–1.75 T, the phase switching between SkX and SkL can be realized through FE transition. It should be noted that upon applying external strain, the bond length and angle would be changed, which could affect the magnetic parameters. Therefore, strain can also be applied to tune the skyrmion physics.[25,50,51]

From the above, we can see that $d_\parallel$ and K play important roles in realizing the topological magnetism. To get a deep insight into their combined effect, we investigated the evolution of spin textures as a function of $d_\parallel$ and K. Fig. 4(a) displays the corresponding phase diagram. We find that a dimensionless parameter $\kappa = \left(\frac{4}{\pi}\right)^2\frac{2JK}{3d_\parallel^2}$ can be used to describe their combined effect on the topological spin texture.[20,34] As shown in Fig. 4(a), for the spin textures around κ = 1, magnetic skyrmions appear around the labyrinth domains. Since $\kappa \propto \frac{K}{d_\parallel^2}$, the larger magnitude of κ ($\gg$ 1) signifies the enhanced spin collinear arrangement, vanishing the labyrinth domains. For κ = 3 and κ = −3, the isolated magnetic skyrmions and

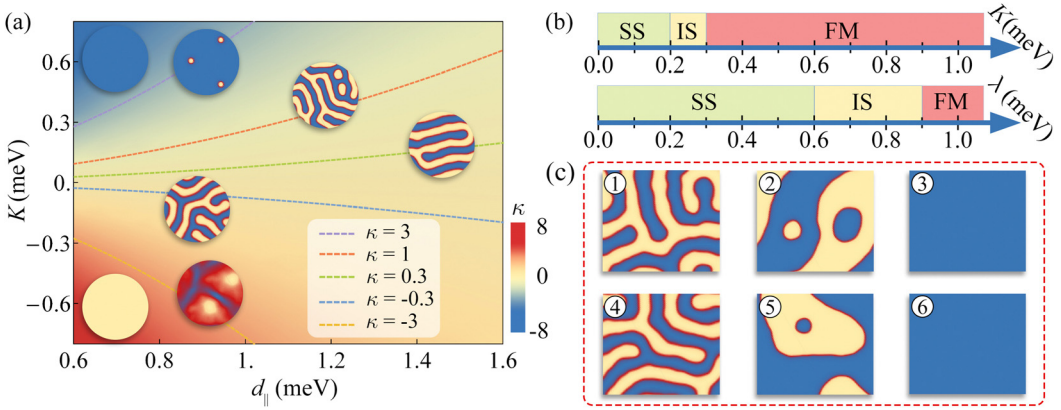

Fig. 4 (a) Spin texture diagram of Co_2NF_2 as a function of $d_\parallel$ and K, wherein J and λ are set to 3.61 and 0 meV, respectively. The gray, orange, green, blue and yellow lines represent κ = 3, 1, 0.3, −0.3 and −3, respectively. The color map specifies the value of κ. (b) Phase diagram of spin textures with K (λ = 0) and λ (K = 0), wherein J and $d_\parallel$ are set to 3.61 and 1.01 meV. IS represents spin textures including isolated magnetic skyrmion. (c) Selected spin textures from (b): K = ① 0.2, ② 0.6, ③ 0.9 meV (λ = 0 meV) and λ = ④ 0.02, ⑤ 0.2, ⑥ 0.3 meV (K = 0 meV).

meron pairs are, respectively, generated along with the reduction of labyrinth domains. With further increasing κ, the topological magnetism will be transformed into the trivial FM phase. For smaller magnitude of κ ($\ll$ 1), the DMI plays a dominated role, giving rise to the SS phase.

To verify the validation of dimensionless parameter κ in assessing the possibility for realizing magnetic skyrmions, we calculate κ for Co_2NF_2 and $Co_2NF_2/MoSe_2$. As shown in Table S1 (ESI†), for Co_2NF_2, κ = 2.3 suggests that a SkX phase is stabilized according to the phase diagram shown in Fig. 4(a), which agrees well with MC simulations. However, according to the phase diagram shown in Fig. 4(a), κ = 1.0 indicates that +P↑ tends to form SkX phase, while κ = 0.6 suggests that −P↓ prefers SkL phase, which is quite different from the MC simulations. This discrepancy stems from the fact that λ is neglected. Fig. 4(b) and (c) display the evolution of spin textures as a function of λ and K, respectively. It can be seen that the ability of λ to enhance collinear arrangement is roughly equivalent to that of triple K. Therefore, we substitute the K term by $K + 3 \times \lambda$ and the expression of κ is transformed into $\kappa' = \left(\frac{4}{\pi}\right)^2 \frac{2J(K+3\lambda)}{3{d_\parallel}^2}$. It should be noted that the elaborations on the phase diagram of κ in Fig. 4(a) remain applicable to κ'. As shown in Table S1 (ESI†), κ' is calculated to be 1.80 for monolayer Co_2NF_2, indicating the stabilization of the SkX phase in the presence of a magnetic field. For $Co_2NF_2/MoSe_2$, +P↑ (κ' = 0.2) tends to form SkL phase, while −P↓ (κ' = 1.0) prefers SkX phase. The calculated κ' agrees well with the MC simulations. Therefore, the dimensionless parameter κ' can be considered as the criteria for assessing the formation of magnetic skyrmions in such multiferroic lattices.

To summarize, we investigate the topological magnetism in 2D multiferroics of Co_2NF_2 on the basis of first-principles calculations and MC simulations. We find that Co_2NF_2 can exhibit magnetic skyrmions under moderate magnetic field, with the size of sub-10 nm. Arising from the magnetoelectric coupling effect, the chirality of magnetic skyrmions in monolayer Co_2NF_2 can be reversed *via* FE transition. Moreover, through interfacing with monolayer $MoSe_2$, the ferroelectric control of more skyrmion properties is realized, such as the creation-annihilation of magnetic skyrmions and the phase transition between SkX and SkL. In addition, we introduce a dimensionless parameter κ' as the criterion for assessing the formation of magnetic skyrmions in such multiferroic lattices.

Conflicts of interest

The authors declare no conflict of interest.

Acknowledgements

This work is supported by the National Natural Science Foundation of China (no. 12274261 and 12074217), Shandong Provincial Science Foundation for Excellent Young Scholars (no. ZR2020YQ04), Shandong Provincial Key Research and Development Program (Major Scientific and Technological Innovation Project) (no. 2019JZZY010302), Shandong Provincial QingChuang Technology Support Plan (no. 2021KJ002), and Taishan Young Scholar Program of Shandong Province.

References

1 B. Göbel, I. Mertig and O. A. Tretiakov, Beyond skyrmions: Review and perspectives of alternative magnetic quasiparticles, *Phys. Rep.*, 2021, **895**, 1.
2 H. Yang, A. Thiaville, S. Rohart, A. Fert and M. Chshiev, Anatomy of Dzyaloshinskii-moriya interaction at Co/Pt interfaces, *Phys. Rev. Lett.*, 2015, **115**, 267210.
3 J. Cho, N. H. Kim, S. Lee, J. S. Kim, R. Lavrijsen, A. Solignac, Y. Yin, D. S. Han, N. J. Van Hoof, H. J. Swagten and B. Koopmans, Thickness dependence of the interfacial Dzyaloshinskii-Moriya interaction in inversion symmetry broken systems, *Nat. Commun.*, 2015, **6**, 1.

4 G. Beutier, S. P. Collins, O. V. Dimitrova, V. E. Dmitrienko, M. I. Katsnelson, Y. O. Kvashnin, A. I. Lichtenstein, V. V. Mazurenko, A. G. A. Nisbet, E. N. Ovchinnikova and D. Pincini, Band filling control of the Dzyaloshinskii-Moriya interaction in weakly ferromagnetic insulators, *Phys. Rev. Lett.*, 2017, **119**, 167201.
5 S. Mühlbauer, B. Binz, F. Jonietz, C. Pfleiderer, A. Rosch, A. Neubauer, R. Georgii and P. Böni, Skyrmion lattice in a chiral magnet, *Science*, 2009, **323**, 915.
6 X. Z. Yu, Y. Onose, N. Kanazawa, J. H. Park, J. H. Han, Y. Matsui, N. Nagaosa and Y. Tokura, Real-space observation of a two-dimensional skyrmion crystal, *Nature*, 2010, **465**, 901.
7 A. N. Bogdanov and C. Panagopoulos, Physical foundations and basic properties of magnetic skyrmions, *Nat. Rev. Phys.*, 2020, **2**, 492.
8 L. Caretta, M. Mann, F. Büttner, K. Ueda, B. Pfau, C. M. Günther, P. Hessing, A. Churikova, C. Klose, M. Schneider and D. Engel, Fast current-driven domain walls and small skyrmions in a compensated ferrimagnet, *Nat. Nanotechnol.*, 2018, **13**, 1154.
9 J. Zang, M. Mostovoy, J. H. Han and N. Nagaosa, Dynamics of skyrmion crystals in metallic thin films, *Phys. Rev. Lett.*, 2011, **107**, 136804.
10 N. Kanazawa, S. Seki and Y. Tokura, Noncentrosymmetric magnets hosting magnetic skyrmions, *Adv. Mater.*, 2017, **29**, 1603227.
11 S. Seki, X. Z. Yu, S. Ishiwata and Y. Tokura, Observation of skyrmions in a multiferroic material, *Science*, 2012, **336**, 198.
12 A. Soumyanarayanan, M. Raju, A. L. Gonzalez Oyarce, A. K. Tan, M. Y. Im, A. P. Petrović, P. Ho, K. H. Khoo, M. Tran, C. K. Gan and F. Ernult, Tunable room-temperature magnetic skyrmions in Ir/Fe/Co/Pt multilayers, *Nat. Mater.*, 2017, **16**, 898.
13 N. Nagaosa and Y. Tokura, Topological properties and dynamics of magnetic skyrmions, *Nat. Nanotechnol.*, 2013, **8**, 899.
14 R. Wiesendanger, Nanoscale magnetic skyrmions in metallic films and multilayers: a new twist for spintronics, *Nat. Rev. Mater.*, 2016, **1**, 1.
15 X. Z. Yu, N. Kanazawa, Y. Onose, K. Kimoto, W. Z. Zhang, S. Ishiwata, Y. Matsui and Y. Tokura, Near room-temperature formation of a skyrmion crystal in thin-films of the helimagnet FeGe, *Nat. Mater.*, 2011, **10**, 106.
16 C. Moreau-Luchaire, C. Moutafis, N. Reyren, J. Sampaio, C. A. F. Vaz, N. Van Horne, K. Bouzehouane, K. Garcia, C. Deranlot, P. Warnicke and P. Wohlhüter, Additive interfacial chiral interaction in multilayers for stabilization of small individual skyrmions at room temperature, *Nat. Nanotechnol.*, 2016, **11**, 444.
17 B. Satywali, V. P. Kravchuk, L. Pan, M. Raju, S. He, F. Ma, A. P. Petrović, M. Garst and C. Panagopoulos, Microwave resonances of magnetic skyrmions in thin film multilayers, *Nat. Commun.*, 2021, **12**, 1.
18 M. G. Han, J. A. Garlow, Y. Liu, H. Zhang, J. Li, D. DiMarzio, M. W. Knight, C. Petrovic, D. Jariwala and Y. Zhu, Topological magnetic-spin textures in two-dimensional van der Waals $Cr_2Ge_2Te_6$, *Nano Lett.*, 2019, **19**, 7859.
19 B. Ding, Z. Li, G. Xu, H. Li, Z. Hou, E. Liu, X. Xi, F. Xu, Y. Yao and W. Wang, Observation of magnetic skyrmion bubbles in a van der Waals ferromagnet Fe_3GeTe_2, *Nano Lett.*, 2019, **20**, 868.
20 J. Liang, W. Wang, H. Du, A. Hallal, K. Garcia, M. Chshiev, A. Fert and H. Yang, Very large Dzyaloshinskii-Moriya interaction in two-dimensional Janus manganese dichalcogenides and its application to realize skyrmion states, *Phys. Rev. B*, 2020, **101**, 184401.
21 C. Xu, J. Feng, S. Prokhorenko, Y. Nahas, H. Xiang and L. Bellaiche, Topological spin texture in Janus monolayers of the chromium trihalides Cr(I, X)3, *Phys. Rev. B*, 2020, **101**, 060404.
22 W. Du, K. Dou, Z. He, Y. Dai, B. Huang and Y. Ma, Spontaneous magnetic skyrmions in single-layer $CrInX_3$ (X= Te, Se), *Nano Lett.*, 2022, **22**, 3440.
23 W. Sun, W. Wang, J. Zang, H. Li, G. Zhang, J. Wang and Z. Cheng, Manipulation of magnetic skyrmion in a 2D van der Waals heterostructure *via* both electric and magnetic fields, *Adv. Funct. Mater.*, 2021, **31**, 2104452.
24 S. Fragkos, P. Pappas, E. Symeonidou, Y. Panayiotatos and A. Dimoulas, Magnetic skyrmion manipulation in CrTe2/WTe2 2D van der Waals heterostructure, *Appl. Phys. Lett.*, 2022, **120**, 182402.
25 D. Li, S. Haldar and S. Heinze, Strain-driven zero-field near-10 nm skyrmions in two-dimensional van der Waals Heterostructures, *Nano Lett.*, 2022, **22**, 7706.
26 M. Schott, A. Bernand-Mantel, L. Ranno, S. Pizzini, J. Vogel, H. Béa, C. Baraduc, S. Auffret, G. Gaudin and D. Givord, The skyrmion switch: turning magnetic skyrmion bubbles on and off with an electric field, *Nano Lett.*, 2017, **17**, 3006.
27 L. Wang, Q. Feng, Y. Kim, R. Kim, K. H. Lee, S. D. Pollard, Y. J. Shin, H. Zhou, W. Peng, D. Lee, W. Meng, H. Yang, J. H. Han, M. Kim, Q. Lu and T. W. Noh, Ferroelectrically tunable magnetic skyrmions in ultrathin oxide heterostructures, *Nat. Mater.*, 2018, **17**, 1087.
28 X. Yu, D. Morikawa, Y. Tokunaga, M. Kubota, T. Kurumaji, H. Oike, M. Nakamura, F. Kagawa, Y. Taguchi, T. Arima, M. Kawasaki and Y. Tokura, Current-induced nucleation and annihilation of magnetic skyrmions at room temperature in a chiral magnet, *Adv. Mater.*, 2017, **29**, 1606178.
29 S. Komineas and N. Papanicolaou, Skyrmion dynamics in chiral ferromagnets under spin-transfer torque, *Phys. Rev. B*, 2015, **92**(17), 174405.
30 P. J. Hsu, A. Kubetzka, A. Finco, N. Romming, K. Von Bergmann and R. Wiesendanger, Electric-field-driven switching of individual magnetic skyrmions, *Nat. Nanotech.*, 2017, **12**, 123.
31 A. Hrabec, J. Sampaio, M. Belmeguenai, I. Gross, R. Weil, S. M. Chérif, A. Stashkevich, V. Jacques, A. Thiaville and S. Rohart, Current-induced skyrmion generation and dynamics in symmetric bilayers, *Nat. Commun.*, 2017, **8**, 1.
32 K. Dou, W. Du, Y. Dai, B. Huang and Y. Ma, Two-dimensional magnetoelectric multiferroics in a $MnSTe/In_2Se_3$ heterobilayer

with ferroelectrically controllable skyrmions, *Phys. Rev. B*, 2022, **105**, 205427.
33 K. Huang, D. F. Shao and E. Y. Tsymbal, Ferroelectric control of magnetic skyrmions in two-dimensional van der Waals heterostructures, *Nano Lett.*, 2022, **22**, 3349.
34 Q. Cui, Y. Zhu, J. Jiang, J. Liang, D. Yu, P. Cui and H. Yang, Ferroelectrically controlled topological magnetic phase in a Janus-magnet-based multiferroic heterostructure, *Phys. Rev. Res.*, 2021, **3**, 043011.
35 J. J. Zhang, L. Lin, Y. Zhang, M. Wu, B. I. Yakobson and S. Dong, Type-II multiferroic $Hf_2VC_2F_2$ MXene monolayer with high transition temperature, *J. Am. Chem. Soc.*, 2018, **140**, 9768.
36 W. Sun, W. Wang, H. Li, G. Zhang, D. Chen, J. Wang and Z. Cheng, Controlling bimerons as skyrmion analogues by ferroelectric polarization in 2D van der Waals multiferroic heterostructures, *Nat. Commun.*, 2020, **11**, 1.
37 C. Huang, J. Zhou, H. Sun, F. Wu, Y. Hou and E. Kan, Toward room-temperature electrical control of magnetic order in multiferroic van der Waals materials, *Nano Lett.*, 2022, **22**, 5191.
38 G. Yu, A. Pan and M. Chen, Interface engineering of ferroelectricity in thin films of thiophosphate ABP_2X_6 (A= Cu, Ag; B= In, Bi, Cr, V; X= S, Se), *Phys. Rev. B*, 2021, **104**, 224102.
39 M. Wu and X. C. Zeng, Intrinsic ferroelasticity and/or multiferroicity in two-dimensional phosphorene and phosphorene analogues, *Nano Lett.*, 2016, **16**, 3236.
40 A. Chandrasekaran, A. Mishra and A. K. Singh, Ferroelectricity, antiferroelectricity, and ultrathin 2D electron/hole gas in multifunctional monolayer MXene, *Nano Lett.*, 2017, **17**, 3290.
41 Y. Fang, S. Wu, Z. Z. Zhu and G. Y. Guo, Large magneto-optical effects and magnetic anisotropy energy in two-dimensional $Cr_2Ge_2Te_6$, *Phys. Rev. B*, 2018, **98**, 125416.
42 P. W. Anderson, Antiferromagnetism. Theory of superexchange interaction, *Phys. Rev.*, 1950, **79**, 350.
43 J. B. Goodenough, Theory of the role of covalence in the perovskite-type manganites [La, M(II)]MnO_3, *Phys. Rev.*, 1955, **100**, 564.
44 J. Kanamori, Superexchange interaction and symmetry properties of electron orbitals, *J. Phys. Chem. Solids*, 1959, **10**, 87.
45 T. Moriya, Anisotropic superexchange interaction and weak ferromagnetism, *Phys. Rev.*, 1960, **120**, 91.
46 A. Fert, N. Reyren and V. Cros, Magnetic skyrmions: advances in physics and potential applications. Nature Reviews, *Materials*, 2017, **2**, 1.
47 B. Berg and M. Lüscher, Definition and statistical distributions of a topological number in the lattice O(3) σ-model, *Nuclear Phys. B*, 1981, **190**, 412.
48 Y. Zhou, Y. Wang, J. Cao, Z. Zeng, T. Zhou, R. Liao, T. Wang, Z. Wang, Z. Xia, Z. Ouyang and H. Lu, $CoMOF_5$(pyrazine)$(H2O)_2$ (M= Nb, Ta): two-layered cobalt oxyfluoride antiferromagnets with spin flop transitions, *Inorg. Chem.*, 2021, **60**, 13309.
49 Z. Shao, J. Liang, Q. Cui, M. Chshiev, A. Fert, T. Zhou and H. Yang, Multiferroic materials based on transition-metal dichalcogenides: Potential platform for reversible control of Dzyaloshinskii-Moriya interaction and skyrmion *via* electric field, *Phys. Rev. B*, 2022, **105**, 174404.
50 F. Zhang, W. Mi and X. Wang, Spin-dependent electronic structure and magnetic anisotropy of 2D ferromagnetic Janus $Cr_2I_3X_3$ (X= Br, Cl) monolayers, *Adv. Electron. Mater.*, 2020, **6**, 1900778.
51 Z. Shen, C. Song, Y. Xue, Z. Wu, J. Wang and Z. Zhong, Strain-tunable Dzyaloshinskii-Moriya interaction and skyrmions in two-dimensional Janus $Cr_2X_3Y_3$ (X, Y= Cl, Br, I, X≠ Y) trihalide monolayers, *Phys. Rev. B*, 2022, **106**, 094403.